THE JOURNAL OF PHYSICAL CHEMISTRY Letters

Letter

pubs.acs.org/JPCL

Catalytic Decomposition of Hydroxylammonium Nitrate Ionic Liquid: Enhancement of NO Formation

Steven D. Chambreau,[†] Denisia M. Popolan-Vaida,[‡,§] Ghanshyam L. Vaghjiani,*[,∥] and Stephen R. Leone[‡,§]

[†]ERC, Inc., Edwards Air Force Base, California 93524, United States

[‡]Departments of Chemistry and Physics, University of California, Berkeley, California 94720, United States

[§]Chemical Sciences Division, Lawrence Berkeley National Laboratory, Berkeley, California 94720, United States

[∥]In-Space Propulsion Branch, Rocket Propulsion Division, Aerospace Systems Directorate, Air Force Research Laboratory, AFRL/RQRS, Edwards Air Force Base, California 93524, United States

Supporting Information

ABSTRACT: Hydroxylammonium nitrate (HAN) is a promising candidate to replace highly toxic hydrazine in monopropellant thruster space applications. The reactivity of HAN aerosols on heated copper and iridium targets was investigated using tunable vacuum ultraviolet photoionization time-of-flight aerosol mass spectrometry. The reaction products were identified by their mass-to-charge ratios and their ionization energies. Products include NH_3, H_2O, NO, hydroxylamine (HA), HNO_3, and a small amount of NO_2 at high temperature. No N_2O was detected under these experimental conditions, despite the fact that N_2O is one of the expected products according to the generally accepted thermal decomposition mechanism of HAN. Upon introduction of iridium catalyst, a significant enhancement of the NO/HA ratio was observed. This observation indicates that the formation of NO via decomposition of HA is an important pathway in the catalytic decomposition of HAN.

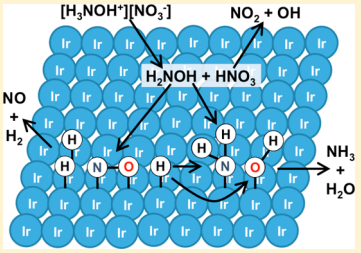

The introduction of hydroxylammonium nitrate (HAN) ionic liquid as a replacement for hydrazine as a spacecraft monopropellant has been of great interest recently due to the reduced toxicity and the improved performance afforded by HAN over hydrazine. HAN is one component of the formulation used in the small demonstration satellite-4 (SDS-4) developed by the Japan Aerospace Exploration Agency,[1] and it is a component of the AF-M315E monopropellant to be used in NASA's Green Propellant Infusion Mission.[2,3] Extensive experimental work has been performed on the thermal decomposition of HAN by Cronin and Brill,[4−8] Oxley and Brower,[9] Lee and Litzinger,[10−12] and Kappenstein et al.[13−15] While much effort has been dedicated to understanding the HAN thermal decomposition mechanism (over 30 publications), only very recently have efforts been made to understand the catalytic decomposition mechanism of HAN in order to optimize the design of HAN-based monopropellant catalysts and thrusters.[1,14−20] A brief summary of the HAN thermal decomposition mechanism is presented here. A detailed overview of the current understanding of both thermal decomposition and catalytic decomposition of HAN can be found elsewhere (in ref 1 and references therein).

Pure, solid HAN is unstable, so HAN is typically stored mixed with H_2O. Upon heating HAN solutions under atmospheric pressure, the first step is an endotherm that vaporizes water. The subsequent decomposition is a two-step exothermic process.[13,18] Decomposition onset temperatures for HAN have been reported in the range of 100−140 °C.[7,9,13,18] The thermal decomposition pathways are presented as a combination of elementary and global reactions that are based on experimental observations:[9]

$$H_3NOH^+NO_3^- \rightarrow H_2NOH + HNO_3 \quad (1)$$

$$H_2NOH + 2HNO_3 \rightarrow 3HNO_2 + H_2O \quad (2)$$

$$H_2NOH + HNO_2 \rightarrow N_2O + 2H_2O \quad (3)$$

$$H_2NOH + HNO_3 \rightarrow NOH + HNO_2 + H_2O \quad (4)$$

$$H_2NOH + NOH \rightarrow N_2 + 2H_2O \quad (5)$$

$$NOH + HNO_3 \rightarrow 2HNO_2 \quad (6)$$

In this mechanism proposed by Oxley and Brower,[9] any NO formation was attributed to its possible formation from decomposition of HNO_2 or HNO_3. The addition of acetate anion retarded HAN decomposition due to reduction in the acidity (i.e., $[HNO_3]$) in the mixture. Reaction 2 has an activation barrier of E_a = 105 kJ/mol and is dominant at low $[NH_2OH]$, while reaction 3 has an E_a = 65 kJ/mol and is dominant at high $[NH_2OH]$.[9] Due to the different tendencies to form contact ion pairs in pure HAN versus aqueous HAN,[7] the decomposition mechanism of pure HAN is believed to be

Received: March 20, 2017
Accepted: April 24, 2017
Published: April 24, 2017

DOI: 10.1021/acs.jpclett.7b00672
J. Phys. Chem. Lett. 2017, 8, 2126−2130

different from that of aqueous HAN decomposition, and catalytic decomposition is likely different from thermal decomposition of both pure HAN and its aqueous solution, HAN(aq). As HAN(aq) is heated, the dielectric constant of water decreases, and there is an increased tendency to form contact ion pairs rather than solvated ions,[7] possibly enhancing decomposition.

Hydroxylamine (H_2NOH) has been demonstrated to decompose completely on heated Ir catalysts at 45 °C, while the exposure of HNO_3 to heated Ir catalysts results in evaporation of HNO_3, indicating that the H_2NOH primary product further decomposes to create ignition conditions in HAN-based propellants.[19] However, the H_2NOH catalytic decomposition products were not identified.

The intent of this investigation is to probe the secondary products of catalytic decomposition of HAN on Ir to identify important intermediate species in the ignition of HAN-based monopropellants. In this investigation, HAN is first aerosolized and introduced into a mass spectrometer equipped with a heated target upon which the aerosol particles are deposited. The targets in this case are copper (to probe thermal decomposition) and iridium (to probe catalytic decomposition). Upon decomposition (that occurs on the order of tens of microseconds), the products are vaporized into the vacuum chamber and rapidly ionized by tunable vacuum ultraviolet photons generated by the synchrotron source at the Chemical Dynamics Beamline 9.0.2 at the Advanced Light Source, Berkeley, CA. The photoions are accelerated and detected as a function of their time-of-flight, yielding both the mass-to-charge ratio of the photoions and their ionization energies (IE) or appearance energies (AE) in the case of parent ion fragmentation. In this way, the initial products can be definitively identified by both their masses and their ionization energies. Details about the experimental setup can be found elsewhere.[21,22]

By tunable vacuum ultraviolet photoionization time-of-flight mass spectrometry, HAN decomposition product masses were detected with mass-to-charge ratios (m/z) of 17, 18, 30, 32, 33, 44, 46 and 63, seen in Figure 1. The primary thermal

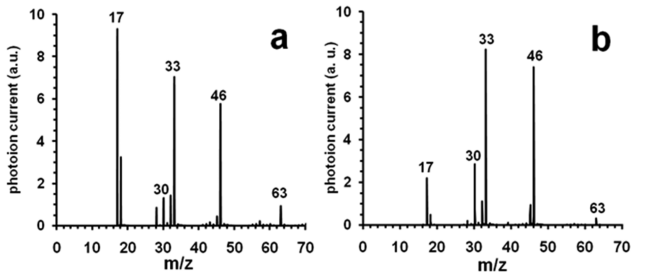

Figure 1. Typical mass spectra at 12.6 eV photoionization energy and a target temperature of 300 °C for (a) the thermal decomposition of HAN on a copper target, and (b) the catalytic decomposition of HAN on an iridium target.

decomposition products (formation of HNO_3 at m/z 63 and H_2NOH at m/z 33 represented by reaction 1) can be seen in Figure 1. Other products observed are formation of NH_3 at m/z 17, H_2O at m/z 18, and the small peak at m/z 30 is identified as NO. While some H_2O is present in the aerosols even after passing the aerosols through a drying tube, a significant increase in H_2O production with increasing target temperature indicates H_2O product formation from HAN catalytic decomposition.

The presence of m/z 46 is assigned to be primarily a fragment of m/z 63 and the peak at m/z 32 is a fragment of HA (m/z 33), and this will be discussed further below. However, a very small amount of the m/z 46 signal can be attributed to the formation of NO_2 at 250 °C and above (also discussed below). Peaks at m/z 28 and 45 are contamination in the mass spectrometer and will not be discussed here. In the limited photon energy range investigated here (8.5−14.5 eV), we do not detect H_2 or N_2, as their IE values are 15.4 and 15.6 eV,[23] respectively. Experimental photoionization energies are determined by fitting the photoionization efficiency curves (PIE) at the photoion onset as described previously[24] (see Figure 2).

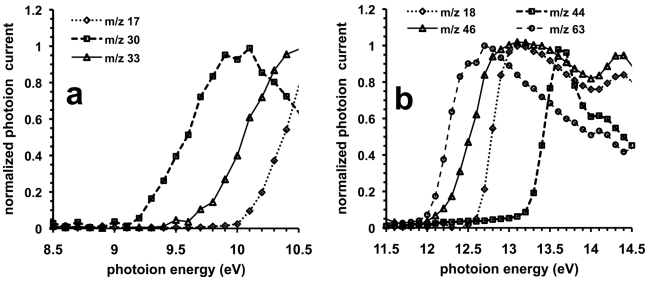

Figure 2. Normalized photoionization efficiency curves for (a) m/z 17, 30, and 33, and for (b) m/z 18, 44, 46, and 63 at 300 °C on the copper target. Photoionization energies are listed in Table 1. Note that separate PIE scans were performed for photon energy ranges from 8.5 to 10.5 eV and 11.5−14.5 eV due to improved signal-to-noise ratios afforded by using a MgF_2 filter from 8.5 to 10.5 eV (MgF_2 is not transparent above 11 eV).

These experimental photoionization energy values (or photoion fragment appearance energies) are presented in Table 1 and are compared to literature values for definitive species identification.

Table 1. Photoion appearance energies

m/z	product	AE/IE[a] (±0.2 eV)	lit AE/IE[b]
17	NH_3	10.0	10.07
18	H_2O	12.6	12.62
30	NO	9.2	9.26
32	frag of HA	12.3	12.34
33	HA	9.6	9.6
44	CO_2	13.3	13.78
46	NO_2	9.2 ± 0.4	9.6
46	frag of HNO_3	12.0	11.90
63	HNO_3	12.0	11.96

[a]This work. [b]Literature values from ref 23.

The observation of photoion peaks at m/z 33 (IE = 9.6 eV) and m/z 63 (IE = 12.0 eV) confirm the production of H_2NOH (HA) and HNO_3, respectively. Another indication of the formation of HA is the appearance of a m/z 32 fragment with an appearance energy AE = 12.3 eV that is very close to the appearance energy of $HNOH^+$ from HA^+ in the literature (12.34 eV).[23] The formation of NH_3 and H_2O is confirmed by their experimental IE values of 10.0 and 12.6 eV, respectively. Production of m/z 30 is identified as NO from its experimental IE = 9.2 eV, which matches well with the literature value of 9.26 eV,[23] and the result is not due to NO^+ fragmentation from NO_2^+, as the NO_2 production is negligible, as discussed below.

DOI: 10.1021/acs.jpclett.7b00672
J. Phys. Chem. Lett. 2017, 8, 2126−2130

The literature IE values for CO_2 and N_2O are 13.777 ± 0.001[23] and 12.889 ± 0.004 eV,[25] respectively. In order to distinguish between CO_2 and N_2O, which both have m/z = 44, each pure gas was individually introduced into the aerosol time-of-flight mass spectrometer (ATOFMS), and photoionization efficiency response curves were measured.[22] In the ATOFMS, the CO_2^+ onset is at 13.3 eV and the PIE has 3 peaks at 13.7, 14.2, and 14.8 eV (see Figure S1, Supporting Information). The N_2O PIE shows a very small signal between 13.2 and 13.6 eV, a significant onset at 13.8 eV that peaks at 14.3 eV, and decays back to the baseline at 15.0 eV. The HAN m/z 44 PIE curve in Figure 2b matches almost exactly, in both peak positions and in peak intensities, with the CO_2 PIE (Figure S1a, Supporting Information), and therefore it is believed that the m/z 44 signal originates exclusively from CO_2^+, the likely source being dissolved CO_2 in the HAN/H_2O mixture used to generate the aerosols. No evidence for the formation of N_2O was observed under these experimental conditions (≤300 °C, 10^{-6} Torr). It would be preferable to use distilled/purged water to make the aerosol solutions or any HAN formulations to avoid dissolved CO_2 contributing to m/z 44 signals observed in electron-impact ionization mass spectrometric investigations of HAN reactivity.

Facile fragmentation of HNO_3^+ is indicated in the literature via reaction 8) below, with an m/z 46 (NO_2^+) AE = 11.90 eV.[23] Since the experimental IE for HNO_3 of 12.0 ± 0.2 eV matches well with the literature value of 11.96 eV, and the fact that, below 250 °C, m/z 46 shows almost no signal below 11.8 eV (Figure 2b), this indicates that the photoions at m/z 46 are almost exclusively from the fragmentation of HNO_3:

$$HNO_3 + h\nu \rightarrow HNO_3^+ + e^- \quad (7)$$

$$HNO_3^+ \rightarrow NO_2^+ + OH \quad (8)$$

It should be noted that, when investigating HAN decomposition using electron-impact ionization mass spectrometry, due to the near simultaneous appearance of HNO_3^+ and its NO_2^+ fragment, in order to detect HNO_3, it is particularly important to use low electron energies so as not to fragment all of the HNO_3^+ from excess internal energy in the initial HNO_3^+ ion. It is also important to determine the extent of fragmentation of the HNO_3^+ ion to NO_2^+ so as to be able to discern the difference between contributions from HNO_3^+ ion fragmentation via reaction 8) and from ionization of any direct NO_2 product.

The possibility of the thermal decomposition of HNO_3 has been proposed[5,10] as

$$HNO_3 \rightarrow NO_2 + OH \quad (9)$$

with an estimated activation energy of $E_a \sim 50$ kcal/mol (~210 kJ/mol).[19] An indication that this is occurring in these experiments is the small increase in the m/z 46 signal below 11 eV (NO_2, IE = 9.6 eV[23]) at temperatures above 250 °C (see Figure S2, Supporting Information). Using the composite method CBS-QB3,[26] reaction 9 is calculated here to have a free energy of reaction of ΔG_{rxn} = 35.4 kcal/mol (148.1 kJ/mol), including zero point vibrational energy, at 298 K and 1 atm. Assuming there is no barrier to the reverse of reaction 9, i.e., $\Delta G_{rxn} = E_a$, it is possible that the NO_2 detected in previous thermal decomposition of HAN experiments could be formed through this route at high temperatures, while also producing the reactive OH radical that can contribute to the proper conditions for the ignition of HAN. Using ΔG_{rxn} = 35.4 kcal/mol (148.1 kJ/mol), it is estimated that reaction 9 can have a percent dissociation of greater than 2% at equilibrium at 300 °C.

The ATOFMS was designed to promote flash vaporization,[21] and, based on previously measured mass loss rates of ionic liquids[27,28] and our measured aerosol mass flow rate into the ATOFMS, the residence and reaction time on the heated targets is estimated to be on the order of tens of microseconds before the volatile initial products are rapidly vaporized into the ionization region at ~10^{-6} Torr. By integrating the photoion current over all photon energies and plotting the product photoion response as a function of target (Cu, Ir) temperature, differences in the thermal decomposition (copper) versus catalytic decomposition chemistry (iridium) can be evaluated (Figure 3). The most significant differences were observed for

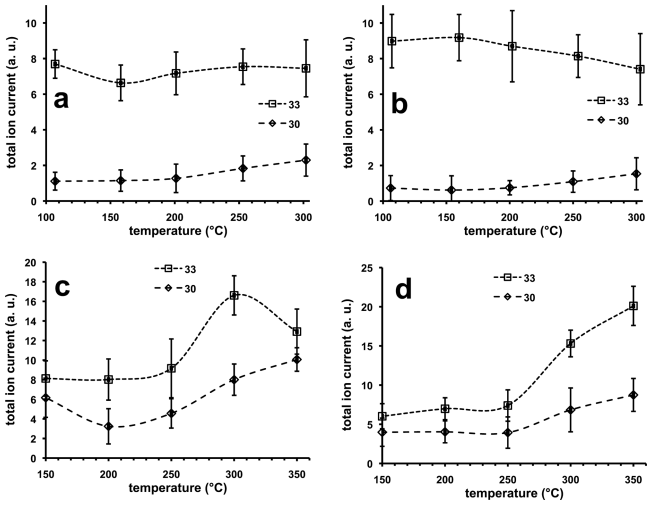

Figure 3. Integrated photoion signals as a function of temperature for m/z 30 (NO) and m/z 33 (HA) on (a) copper, 8.5−10.5 eV, (b) copper, 11.5−14.5 eV, (c) iridium, 8.5−10.5 eV, and (d) iridium, 11.5−14.5 eV. The dashed lines are drawn only to guide the eye of the reader.

product species m/z 30 (NO) and m/z 33 (HA). In the case of thermal decomposition on the copper target, the response ratio of m/z 30/33, i.e., NO/HA was approximately 1:8 at all temperatures investigated. When the copper target is replaced with the iridium target, the NO/HA ratio increases about four times to ~1:2, indicating decomposition of HA to form NO. These experiments were performed twice each to confirm reproducibility. It is interesting to note that for the case of thermal decomposition, the temperature response curves for both HA and NO are relatively flat as the temperature increases, with perhaps a slight decrease in HA response at the higher temperatures when integrated from 11.5 to 14.5 eV. For the case of catalytic decomposition, both the HA and NO signals increase significantly above 250 °C. This could potentially be explained by a catalytic effect on both the initial HAN proton transfer step (see Figure S3, Supporting Information) and on the subsequent HA decomposition. One possible interaction of HA with the iridium catalyst is to strip the hydrogens from the molecule resulting in NO formation:

$$H_2NOH \rightarrow NO + 3/2H_2 \quad (10)$$

Similar hydrogen removal/migration has been proposed for hydrazine (N_2H_4) on iridium, where the N−N bond remains intact and hydrogens can be transferred to the iridium

DOI: 10.1021/acs.jpclett.7b00672
J. Phys. Chem. Lett. 2017, 8, 2126−2130

surface.[29] The irridium catalyst surface can perhaps stabilize radical-type species,[29] thereby lowering the transition state(s) involved in hydrogen loss relative to Cu or bulk solution. The formation of NO, which is itself an open-shell species, could provide an alternative pathway to HNO formation in the gas phase via H-abstraction by NO, thereby promoting radical−neutral and radical−radical reactions that could promote ignition.

Understanding the catalytic reaction chemistry of HAN on iridium is very important to the propulsion community, and these results will help to guide the refinement of the chemical kinetics models used to simulate the ignition and combustion characteristics of next-generation monopropellant thrusters. The enhanced formation of NO by way of H loss on the iridium catalyst appears to be of significant importance in the initial reaction (on the order of tens of microseconds), while N_2O formation is not significant under these experimental conditions, as the time scales are too short and the initial product concentrations are too low to form the secondary product N_2O. Formation of NO_2 by high-temperature thermal decomposition of HNO_3 is supported by these findings, and the coproduction of OH could be important in HAN ignition. Additional work such as reactive scattering of HA on a hot iridium surface and a theoretical study of HAN and HA on iridium clusters (similar to the work of Schmidt and Gordon with hydrazine on iridium)[29] would greatly add to the understanding of the enhanced production of NO from the catalytic decomposition of HAN on iridium.

■ ASSOCIATED CONTENT

Supporting Information

The Supporting Information is available free of charge on the ACS Publications website at DOI: 10.1021/acs.jpclett.7b00672.

PIE curves for CO_2 and N_2O (Figure S1), temperature response curve and PIE curve for NO_2 (Figure S2) and temperature response curve for HNO_3 (Figure S3) (PDF)

■ AUTHOR INFORMATION

Corresponding Author

*E-mail: ghanshyam.vaghjiani@us.af.mil; Tel: 661-275-5657; Fax: 661-275-5203.

ORCID

Ghanshyam L. Vaghjiani: 0000-0001-7473-7388

Stephen R. Leone: 0000-0003-4006-2292

Notes

The authors declare no competing financial interest.

■ ACKNOWLEDGMENTS

The authors gratefully acknowledge funding from the U.S. Air Force Office of Scientific Research for supporting S.R.L. (Grant Nos. FA9550-10-1-0163 and FA9550-14-0154), and S.D.C. (Grant No. FA9300-06-C-0023). The work carried out at the ALS was supported by the Director, Office of Energy Research, Office of Basic Energy Sciences, Chemical Sciences Division of the U.S. Department of Energy under Contract No. DE-AC02-05CH11231 (D.M.P.-V. and S.R.L.). D.M.P.-V. is also particularly grateful to the Alexander von Humboldt Foundation for a Feodor Lynen Fellowship.

■ REFERENCES

(1) Amrousse, R.; Katsumi, T.; Azuma, N.; Hori, K. Hydroxylammonium Nitrate (HAN)-Based Green Propellant as Alternative Energy Resource for Potential Hydrazine Substitution: From Lab Scale to Pilot Plant Scale-Up. *Combust. Flame* **2017**, *176*, 334−348.

(2) NASA GPIM. https://www.nasa.gov/mission_pages/tdm/green/overview.html (accessed January 12, 2017).

(3) David, L. Space.com GPIM. http://www.space.com/32567-nasa-green-propellant-mission-gpim.html (accessed January 12, 2017).

(4) Cronin, J. T.; Brill, T. B. Thermal Decomposition of Energetic Materials. 8. Evidence of an Oscillating Process During the High-Rate Thermolysis of Hydroxylammonium Nitrate, and Comments on the Interionic Interactions. *J. Phys. Chem.* **1986**, *90*, 178−181.

(5) Brill, T. B.; Russell, T. P. Rapid-Scan Infrared/Thermal Profiling Studies Of The Thermal Decomposition Of Selected Nitrate Salts Of Interest For Emulsified Propellants. *Proc. SPIE* **1988**, 40−43.

(6) Cronin, J. T.; Brill, T. B. Thermal Decomposition of Energetic Materials 29. The Fast Thermal Decomposition Characteristics of a Multicomponent Material: Liquid Gun Propellant 1845. *Combust. Flame* **1988**, *74*, 81−89.

(7) Brill, T. B.; Spohn, P. D.; Cronin, J. T. Thermal Decomposition of Energetic Materials 32. On the Instantaneous Molecular Nature of Aqueous Liquid Gun Propellants at High Temperature and Pressure Before Thermal Decomposition. *J. Energ. Mater.* **1990**, *8*, 75−84.

(8) Schoppelrei, J. W.; Brill, T. B. Spectroscopy of Hydrothermal Reactions 7. Kinetics of Aqueous $[NH_3OH]NO_3$ at 463−523 K and 27.5 MPa by Infrared Spectroscopy. *J. Phys. Chem. A* **1997**, *101*, 8593−8596.

(9) Oxley, J. C.; Brower, K. R. Thermal Decomposition Of Hydroxylamine Nitrate. *Proc. SPIE* **1988**, 63−70.

(10) Lee, Y. J.; Litzinger, T. A. Combustion Chemistry of HAN, TEAN, and XM46. *Combust. Sci. Technol.* **1999**, *141*, 19−36.

(11) Lee, H.; Litzinger, T. A. Thermal Decomposition of HAN-Based Liquid Propellants. *Combust. Flame* **2001**, *127*, 2205−2222.

(12) Lee, H.; Litzinger, T. A. Chemical Kinetic Study of HAN Decomposition. *Combust. Flame* **2003**, *135*, 151−169.

(13) Kappenstein, C.; Courthéoux, L.; Eloirdi, R.; Rossignol, S.; Duprez, D.; Pillet, N. Catalytic Decomposition of HAN−Water Binary Mixtures, *38th AIAA/ASME/SAE/ASEE Joint Propulsion Conference & Exhibit, Joint Propulsion Conferences*, American Institute of Aeronautics and Astronautics: Reston, VA, 2002.

(14) Courthéoux, L.; Amariei, D.; Rossignol, S.; Kappenstein, C. Thermal and Catalytic Decomposition of HNF and HAN Liquid Ionic as Propellants. *Appl. Catal., B* **2006**, *62*, 217−225.

(15) Amariei, D.; Courthéoux, L.; Rossignol, S.; Kappenstein, C. Catalytic and Thermal Decomposition of Ionic Liquid Monopropellants Using a Dynamic Reactor: Comparison of Powder and Sphere-Shaped Catalysts. *Chem. Eng. Process.* **2007**, *46*, 165−174.

(16) Banerjee, S.; Shetty, S. A.; Gowrav, M. N.; Oommen, C.; Bhattacharya, A. Adsorption and Decomposition of Monopropellant Molecule HAN on Pd(100) and Ir(100) Surfaces: A DFT Study. *Surf. Sci.* **2016**, *653*, 1−10.

(17) Oommen, C.; Rajaraman, S.; Chandru, R. A.; Rajeev, R. Catalytic Decomposition of Hydroxylammonium Nitrate Monopropellant. *IPCBEE* **2011**, *10*, 205−209.

(18) Amrousse, R.; Hori, K.; Fetimi, W.; Farhat, K. HAN and ADN as Liquid Ionic Monopropellants: Thermal and Catalytic Decomposition Processes. *Appl. Catal., B* **2012**, *127*, 121−128.

(19) Amrousse, R.; Katsumi, T.; Itouyama, N.; Azuma, N.; Kagawa, H.; Hatai, K.; Ikeda, H.; Hori, K. New HAN-Based Mixtures for Reaction Control System and Low Toxic Spacecraft Propulsion Subsystem: Thermal Decomposition and Possible Thruster Applications. *Combust. Flame* **2015**, *162*, 2686−2692.

(20) Amrousse, R.; Katsumi, T.; Niboshi, Y.; Azuma, N.; Bachar, A.; Hori, K. Performance and Deactivation of Ir-Based Catalyst During Hydroxylammonium Nitrate Catalytic Decomposition. *Appl. Catal., A* **2013**, *452*, 64−68.

(21) Koh, C. J.; Liu, C.-L.; Harmon, C. W.; Strasser, D.; Golan, A.; Kostko, O.; Chambreau, S. D.; Vaghjiani, G. L.; Leone, S. R. Soft

DOI: 10.1021/acs.jpclett.7b00672
J. Phys. Chem. Lett. 2017, 8, 2126−2130

Ionization of Thermally Evaporated Hypergolic Ionic Liquid Aerosols. *J. Phys. Chem. A* **2011**, *115*, 4630−4635.
(22) Chambreau, S. D.; Koh, C. J.; Popolan-Vaida, D. M.; Gallegos, C. J.; Hooper, J. B.; Bedrov, D.; Vaghjiani, G. L.; Leone, S. R. Flow-Tube Investigations of Hypergolic Reactions of a Dicyanamide Ionic Liquid Via Tunable Vacuum Ultraviolet Aerosol Mass Spectrometry. *J. Phys. Chem. A* **2016**, *120*, 8011−8023.
(23) Lias, S. G. Ionization Energy Evaluation. In *NIST Chemistry WebBook, NIST Standard Reference Database Number 69*; Linstrom, P. J.; Mallard, W. G., Eds.; National Institute of Standards and Technology: Gaithersburg, MD; http://webbook.nist.gov (retrieved January 4, 2017).
(24) Strasser, D.; Goulay, F.; Belau, L.; Kostko, O.; Koh, C.; Chambreau, S. D.; Vaghjiani, G. L.; Ahmed, M.; Leone, S. R. Tunable Wavelength Soft Photoionization of Ionic Liquid Vapors. *J. Phys. Chem. A* **2010**, *114*, 879−883.
(25) Berkowitz, J.; Eland, J. H. D. Photoionization of N_2O: Mechanisms of Photoionization and Ion Dissociation. *J. Chem. Phys.* **1977**, *67*, 2740−2752.
(26) Petersson, G. A. Complete Basis Set Models for Chemical Reactivity: From the Helium Atom to Enzyme Kinetics. In *Quantum-Mechanical Prediction of Thermochemical Data*; Cioslowski, J., Ed.; Springer: Netherlands: Dordrecht, 2001; pp 99−130 http://dx.doi.org/10.1007/0-306-47632-0_4.
(27) Chambreau, S. D.; Boatz, J. A.; Vaghjiani, G. L.; Koh, C.; Kostko, O.; Golan, A.; Leone, S. R. Thermal Decomposition of 1-Ethyl-3-methylimidazolium Bromide Ionic Liquid. *J. Phys. Chem. A* **2012**, *116*, 5867−5876.
(28) Chambreau, S. D.; Schenk, A. C.; Sheppard, A. J.; Yandek, G. R.; Vaghjiani, G. L.; Maciejewski, J.; Koh, C. J.; Golan, A.; Leone, S. R. Thermal Decomposition Mechanisms of Alkylimidazolium Ionic Liquids with Cyano-Functionalized Anions. *J. Phys. Chem. A* **2014**, *118*, 11119−11132.
(29) Schmidt, M. W.; Gordon, M. S. The Decomposition of Hydrazine in the Gas Phase and over an Iridium Catalyst. *Z. Phys. Chem.* **2013**, *227*, 1301−1306.

DOI: 10.1021/acs.jpclett.7b00672
J. Phys. Chem. Lett. 2017, 8, 2126−2130